Cosmic Microwave Background Theory

J. Richard Bond
CIAR Cosmology Program, Canadian Institute for Theoretical Astrophysics,
60 St. George St., Toronto, ON M5S 3H8, Canada

ABSTRACT A long-standing goal of theorists has been to constrain cosmological parameters that define the structure formation theory from CMB anisotropy experiments and large scale structure (LSS) observations. The status and future promise of this enterprise is described. Current band-powers in ℓ-space are consistent with a ΔT flat in frequency and broadly follow inflation-based expectations. That the levels are $\sim (10^{-5})^2$ provides strong support for the gravitational instability theory, while the FIRAS constraints on energy injection rule out cosmic explosions as a dominant source of large scale structure. Band-powers at $\ell \gtrsim 100$ suggest the universe could not have reionized too early. To get the LSS of COBE-normalized fluctuations right provides encouraging support that the initial fluctuation spectrum was not far off the scale invariant form that inflation models prefer: *e.g.*, for tilted ΛCDM sequences of fixed 13 Gyr age (with H_0 marginalized), $n_s = 1.17 \pm 0.3$ for DMR only; 1.15 ± 0.08 for DMR plus the SK95 experiment; 1.00 ± 0.04 for DMR plus all smaller angle experiments; 1.00 ± 0.05 when LSS constraints are included as well. The CMB alone currently gives weak constraints on Λ and moderate constraints on Ω_{tot}, but theoretical forecasts of future long duration balloon and satellite experiments are shown which predict percent-level accuracy among a large fraction of the 10+ parameters characterizing the cosmic structure formation theory, at least if it is an inflation variant.

I. THE THEORETICAL AGENDA

A. CMB as a Probe of Early Universe Physics

The source of fluctuations to input into the cosmic structure formation problem is likely to be found in early universe physics. We want to measure the CMB (and large scale structure) response to these initial fluctuations. The goal is the lofty one of peering into the physical mechanism by which the fluctuations were generated. The contenders for generation mechanism are (1) "zero point" quantum noise in scalar and tensor fields that must be there in the early universe if quantum mechanics is applicable and (2) topological defects which may arise in the inevitable phase transitions expected in the early universe.

From CMB and LSS observations we hope to learn: the statistics of the fluctuations, whether Gaussian or non-Gaussian; the mode, whether adiabatic or isocurvature scalar perturbations, and whether there is a significant component in gravitational wave tensor perturbations; the power spectra for these modes, $\mathcal{P}_\Phi(k), \mathcal{P}_{is}(k), \mathcal{P}_{GW}(k)$ as a function of comoving wavenumber k. Sample initial and evolved power spectra for the gravitational potential $\mathcal{P}_\Phi(k)$ ($\equiv d\sigma_\Phi^2/d\ln k$, the *rms* power in each $d\ln k$ band) are shown in Fig. 1. As the Universe evolves the initial shape of $\mathcal{P}_\Phi$ is modified by characteristic scales imprinted on it that reflect the values of cosmological parameters such as the energy densities of baryons, cold and hot dark matter, in the vacuum (cosmological constant), and in curvature. Many observables can be expressed as weighted integrals over k of the power specta and thus can probe both density parameters and initial fluctuation parameters.

The (linear) density power spectra, $\mathcal{P}_\rho(k) \propto k^4 \mathcal{P}_\Phi(k)$, are also shown in Fig. 1. In hierarchical structure formation models such as those considered here, the nonlinear wavenumber $k_{NL}(t)$, defined by $\int_0^{k_{NL}} \mathcal{P}_\rho(k) d\ln k = 1$, grows as the universe expands. $k_{NL}(t)$ was in the galaxy band at redshift 3 and is currently in the cluster band. At $k > k_{NL}(t)$, nonlinearities and complications associated with dissipative gas processes can obscure the direct connection to the early universe physics. Most easily interpretable are observables probing the linear regime now, $k < k_{NL}(t_0)$. CMB anisotropies arising from the linear regime are termed primary; as Fig. 1 shows, these probe 3 decades in wavenumber. LSS observations at low redshift probe a smaller, but overlapping, range. We have hope that $z \sim 3$ LSS observations, when $k_{NL}(t)$ was larger, can extend the range, but gasdynamics can modify the relation between observable and power spectrum in complex ways. Secondary anisotropies of the CMB (§ IF), those associated with nonlinear phenomena, also probe smaller scales and the "gastrophysical" realm.

B. Cosmic Parameters

Even simple Gaussian inflation-generated fluctuations for structure formation have a large number of early universe parameters we would wish to

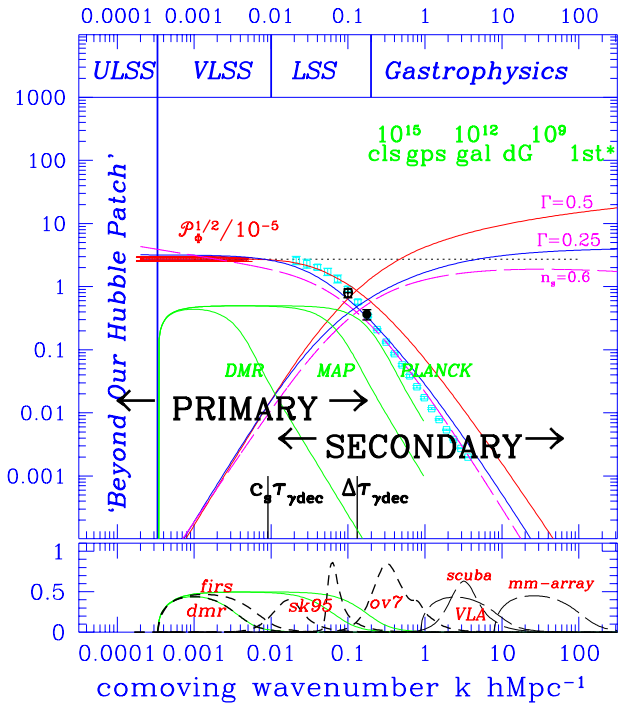

FIG. 1. The bands in comoving wavenumber k probed by CMB primary and secondary anisotropy experiments, in particular by the satellites COBE, MAP and Planck, and by large scale structure (LSS) observations are contrasted. The width of the CMB photon decoupling region and the sound crossing radius $(\Delta\tau_{\gamma dec}, c_s\tau_{\gamma dec})$ define the effective acoustic peak range. Sample (linear) gravitational potential power spectra (actually $\mathcal{P}_\Phi^{1/2}(k)$) are also plotted. The hatched region at low k gives the 4 year DMR error bar on the Φ amplitude in the COBE regime. The solid data point in the cluster-band denotes the Φ constraint from the abundance of clusters, and the open data point at $10\,h^{-1}$ Mpc a Φ constraint from streaming velocities (for Ω_{tot}=1,Ω_Λ=0). The open squares are estimates of the linear Φ power from current galaxy clustering data by [5]. A bias is "allowed" to (uniformly) raise the shapes to match the observations. The corresponding linear density power spectra, $\mathcal{P}_\rho^{1/2}(k)$, are also shown rising to high k: Models are the "standard" $n_s = 1$ CDM model (labelled $\Gamma = 0.5$), a tilted ($n_s = 0.6$, $\Gamma = 0.5$) CDM model and a model with the shape modified ($\Gamma = 0.25$) by changing the matter content of the Universe.

determine (§ IC): power spectrum amplitudes at some normalization wavenumber k_n for the modes present, $\{\mathcal{P}_\Phi(k_n), \mathcal{P}_{is}(k_n), \mathcal{P}_{GW}(k_n)\}$; shape functions for the "tilts" $\{\nu_s(k), \nu_{is}(k), \nu_t(k)\}$, usually chosen to be constant or with a logarithmic correction, e.g., $\nu_s(k_n), d\nu_s(k_n)/d\ln k$. (The scalar tilt for adiabatic fluctuations, $\nu_s(k) \equiv d\ln\mathcal{P}_\Phi/d\ln k$, is related to the usual index, n_s, by $\nu_s = n_s - 1$.) The transport problem (§ IE) is dependent upon physical processes, and hence on physical parameters. A partial list includes the Hubble parameter h, various mean energy densities $\{\Omega_{tot}, \Omega_B, \Omega_\Lambda, \Omega_{cdm}, \Omega_{hdm}\}h^2$, and parameters characterizing the ionization history of the Universe, e.g., the Compton optical depth τ_C from a reheating redshift z_{reh} to the present. Instead of Ω_{tot}, we prefer to use the curvature energy parameter, $\Omega_k \equiv 1 - \Omega_{tot}$, thus zero for the flat case. In this space, the Hubble parameter, $h = (\sum_j(\Omega_j h^2))^{1/2}$, and the age of the Universe, t_0, are functions of the $\Omega_j h^2$. The density in nonrelativistic (clustering) particles is $\Omega_{nr} = \Omega_B + \Omega_{cdm} + \Omega_{hdm}$. The density in relativistic particles, Ω_{er}, includes photons, relativistic neutrinos and decaying particle products, if any. Ω_{er}, the abundance of primordial helium, etc. should also be considered as parameters to be determined. The count is thus at least 17. Estimates of errors on a smaller 9 parameter inflation set for the MAP and Planck satellites are given in § IIE.

The arena in which CMB theory battles observation is the anisotropy power spectrum in multipole space, Fig. 2, which shows how primary $\mathcal{C}_\ell$'s vary with some of these cosmic parameters. Here $\mathcal{C}_\ell \equiv \ell(\ell+1)\langle|(\Delta T/T)_{\ell m}|^2\rangle/(2\pi)$. The $\mathcal{C}_\ell$'s are normalized to the 4-year *dmr*(53+90+31)(A+B) data [3,1,4]. The arena for LSS theory is the $\mathcal{P}_\rho$ of Fig. 1.

For a given model, the early universe $\mathcal{P}_\Phi$ is uniquely related to late-time power spectrum measures of relevance for the CMB, such as the quadrupole $\mathcal{C}_2^{1/2}$ or averages over ℓ-bands B, $\langle\mathcal{C}_\ell\rangle_B^{1/2}$, and to LSS measures, such as the *rms* density fluctuation level on the $8\,h^{-1}$ Mpc (cluster) scale, σ_8, so any of these can be used in place of the primordial power amplitudes in the parameter set. In inflation, the ratio of gravitational wave power to scalar adiabatic power is $\mathcal{P}_{GW}/\mathcal{P}_\Phi \approx -(100/9)\nu_t/(1-\nu_t/2)$, with small corrections depending upon $\nu_s - \nu_t$ [1,2]. If such a relationship is assumed, the parameter count is lowered by one.

C. Freedom in Inflation

Many variants of the basic inflation theme have been proposed, sometimes with radically different consequences for $\mathcal{P}_\Phi(k) \sim k^{1-n_s(k)}$, and thus for the CMB sky, which is used in fact to highly constrain the more baroque models. A rank-ordering of inflation possibil-

ities: (1) adiabatic curvature fluctuations with nearly uniform scalar tilt over the observable range, slightly more power to large scales ($0.8 \lesssim n_s \lesssim 1$) than "scale invariance" ($n_s = 1$) gives, a predictable nonzero gravity wave contribution with tilt similar to the scalar one, and tiny mean curvature ($\Omega_{tot} \approx 1$); (2) same as (1), but with a tiny gravity wave contribution; (3) same as (1) but with a subdominant isocurvature component of nearly scale invariant tilt (the case in which isocurvature dominates is ruled out); (4) radically broken scale invariance with weak to moderate features (ramps, mountains, valleys) in the fluctuation spectrum (strong ones are largely ruled out); (5) radical breaking with non-Gaussian features as well; (6) "open" inflation, with quantum tunneling producing a negatively-curved (hyperbolic) space which inflates, but not so much as to flatten the mean curvature ($d_c \sim (Ha)^{-1}$, not $\gg (Ha)^{-1}$, where $d_c \equiv H_0^{-1}|\Omega_k|^{-1/2}$); (7) quantum creation of compact hyperbolic space from "nothing" with volume d_T^3 which inflates, with $d_T \sim (Ha)^{-1}$, not $\gg (Ha)^{-1}$, and d_T of order d_c; (8) flat ($d_c = \infty$) inflating models which are small tori of scale d_T with d_T a few $(Ha)^{-1}$ in size. It is quite debatable which of the cases beyond (2) are more or less plausible, with some claims that (4) is supersymmetry-inspired, others that (6) is not as improbable as it sounds. It is the theorists' job to push out the boundaries of the inflation idea and use the data to select what is allowed.

D. LSS Constraints on the Power Spectrum

We have always combined CMB and LSS data in our quest for viable models. Fig. 1 shows how the two are connected. DMR normalization precisely determines σ_8 for each model considered; comparing with the $\sigma_8 \sim 0.6\Omega_{nr}^{-0.56}$ target value derived from cluster abundance observations severely constrains the cosmological parameters defining the models. In Fig. 1, this means the COBE-normalized $\mathcal{P}_\Phi(k)$ must thread the "eye of the needle" in the cluster-band.

Similar constrictions arise from galaxy-galaxy and cluster-cluster clustering observations: the shape of the linear $\mathcal{P}_\Phi$ must match the shape reconstructed from the data. The reconstruction shown is from [5]. The clustering observations are roughly compatible with an allowed range $0.15 \lesssim \Gamma + \nu_s/2 \lesssim 0.3$, where $\Gamma \approx \Omega_{nr}\,\mathrm{h}\,[\Omega_{er}/(1.68\Omega_\gamma)]^{-1/2}\,e^{-(\Omega_B(1+\Omega_{nr}^{-1}(2\mathrm{h})^{1/2})-0.06)}$ characterizes the density transfer function shape. The SCDM model has $\Gamma \approx 0.5$. To get $\Gamma + \nu_s/2$ in the observed range one can: lower h, lower Ω_{nr} (ΛCDM, OCDM), raise Ω_{er}, the density parameter in relativistic particles ($1.68\Omega_\gamma$ with 3 species of massless neutrinos and the photons), e.g., as in τCDM, with a decaying ν of lifetime τ_d and $\Gamma \approx 1.08\Omega_{nr}\mathrm{h}(1 + 0.96(m_\nu\tau_d/\mathrm{keV\ yr})^{2/3})^{-1/2}$; raise Ω_B; tilt $\nu_s < 0$ (TCDM), for standard CDM parameters, e.g., $0.3 \lesssim n_s \lesssim 0.7$ would be required. Adding a hot dark matter component gives a power spectrum characterized by more than just Γ.

E. Cosmological Radiative Transport

Cosmological radiative transfer is on a firm theoretical footing. Together with a gravity theory (invariably Einstein's general relativity, but the CMB will eventually be used as a test of the gravity theory) and the transport theory for the other fields and particles present (baryons, hot, warm and cold dark matter, coherent fields, i.e., "dynamical" cosmological "constants", *etc.*), we propagate initial fluctuations from the early universe through photon decoupling into the (very) weakly nonlinear phase, and predict *primary anisotropies*, those calculated using either linear perturbation theory (e.g., for inflation-generated fluctuations), or, in the case of defects, linear response theory. The sources driving their development are all proportional to the gravitational potential Φ: the "naive" Sachs-Wolfe effect, $\Phi/3$; photon bunching (acoustic), $\frac{1}{4}\frac{\delta\rho_\gamma}{\rho_\gamma}$, responsible for the adiabatic $\frac{1}{3}\frac{\delta\rho_B}{\rho_B}$ effect and the isocurvature effect; linear-order Thompson scattering (Doppler), $\sigma_T\bar{n}_e\mathbf{v}_e\cdot\hat{q}$, with σ_T the Thomson cross section, $\mathbf{v}_e$ and $\bar{n}_e$ the electron velocity and density, and $\hat{q}$ the photon direction; the (line-of-sight) integrated Sachs-Wolfe effect, $\sim 2\int_{l.o.s.}\dot{\Phi}$; there are also subdominant anisotropic stress and polarization terms. For primary tensor anisotropies, the sources are the two polarization states of gravity waves, $\frac{1}{2}\dot{h}_{+,\times}$; again there are subdominant polarization terms.

Spurred on by the promise of percent-level precision in cosmic parameters from CMB satellites (§ II E), a considerable fraction of the CMB theoretical community with Boltzmann transport codes compared their approaches and validated the results to ensure percent-level accuracy up to $\ell \sim 3000$ (COMBA [6]). An important goal for COMBA was speed, since the parameter space we wish to constrain has many dimensions. Most groups have solved cosmological radiative transport by evolving a hierarchy of coupled moment equations, one for each ℓ. Although the equations and techniques were in place prior to the COBE discovery for scalar modes, and shortly after for tensor modes, to get the high accuracy with speed has been somewhat of a challenge. There are alternatives to the moment hierarchy for the transport of photons and neutrinos. In particular the entire problem of photon transport reduces to integral equations in which the multipoles with $\ell > 2$ are expressed as history-integrals of metric variables, photon-bunching, Doppler and polarization sources. The fastest COMBA-validated code uses this method [7].

F. Secondary Anisotropies

Although hydrodynamic and radiative processes are expected to play important roles around collapsed objects and may bias the galaxy distribution relative to the mass (*gastrophysics* regime in Fig. 1), a global role in obscuring the early universe fluctuations by late time generation on large scales now seems unlikely. Not too long ago it seemed perfectly reasonable based on extrapolation from the physics of the interstellar medium to the pregalactic and intergalactic medium to suppose hydrodynamical amplification of seed cosmic structure could create the observed Universe. The strong limits on Compton cooling from FIRAS [8], in energy $\delta E_{Compton\ cool}/E_{cmb} = 4y < 6.0 \times 10^{-5}$ (95% CL), constrain the product $f_{exp}R_{exp}^2$ of filling factor f_{exp} and bubble formation scale R_{exp}, to values too small for a purely hydrodynamic origin. If supernovae were responsible for the blasts, the accompanying presupernova light radiated would have been much in excess of the explosive energy (more than a hundred-fold), leading to much stronger restrictions (e.g., [1]).

Nonetheless significant "secondary anisotropies" are expected. These include: linear weak lensing, dependent on the 2D (projected) tidal tensor, ε_{AB}; the Rees-Sciama effect, $2\int_{l.o.s.}\dot{\Phi}_{NL}$, dependent upon the gravitational potential changes associated with nonlinear structure formation; nonlinear Thompson scattering, $\sigma_T\delta n_e \mathbf{v}_e \cdot \hat{q}$, dependent upon the fluctuation in the electron density δn_e as well as $\mathbf{v}_e$, and responsible for the quadratic-order (Vishniac) effect and the "kinematic" Sunyaev-Zeldovich (SZ) effect (moving cluster/galaxy effect); the thermal SZ effect, associated with Compton cooling, $\int_{l.o.s.}\psi_K(x)\delta(n_eT_e)$, where $\psi_K(x)$ is a function of $x = E_\gamma/T_\gamma$ passing from -2 on the Rayleigh-Jeans end to x on the Wein end, with a null at $x = 2.83$ (i.e., 1863μm or 161 GHz); pregalactic or galactic dust emission, $\sim \int_{l.o.s.}\psi_{dust}(x_d)\rho_d$, dependent upon the distribution of the dust density ρ_d and temperature T_d through a function of $x_d = E_\gamma/T_d$.

Secondary anisotropies may be considered as a nuisance foreground to be subtracted to get at the primary ones, but they are also invaluable probes of shorter-distance aspects of structure formation theories, full of important cosmological information. The k-space range they probe is shown in Fig. 1. The effect of lensing is to smooth slightly the Doppler peaks and troughs of Fig. 2. $\mathcal{C}_\ell$'s from quadratic nonlinearities in the gas at high redshift are concentrated at high ℓ, but for most viable models are expected to be a small contaminant. Thomson scattering from gas in moving clusters also has a small effect on $\mathcal{C}_\ell$ (although it should be measurable in individual clusters). Power spectra for the thermal SZ effect from clusters are larger [9]; examples in the top panel of Fig. 2 are for cluster-normalized HCDM and TCDM models, with $\bar{y} \sim (0.5-1)\times 10^{-6}$. OCDM and ΛCDM models have slightly higher values, but still small *c.f.* the FIRAS constraint. Although $\mathcal{C}_\ell^{(SZ)}$ may be small, because the power for such non-Gaussian sources is concentrated in hot or cold spots the signal is detectable, and has been for two dozen clusters now at the > 5 sigma level. $\mathcal{C}_\ell$ for a typical dusty primeval galaxy model is also shown, the smaller angle part (arbitrarily normalized) a shot-noise effect for galaxies with dust distributed over 10 kpc, the larger angle contribution associated with clustering. Dusty anisotropies are very likely to be observable with new instrumentation on submm telescopes (e.g., SCUBA on the James Clerk Maxwell Telescope on Mauna Kea). Similar shot-noise spectra are expected for other extragalactic point sources, e.g., radio galaxies.

II. CMB PARAMETER ESTIMATION, CURRENT AND FUTURE

A. The Theorists' Phenomenology of CMB Experiments

We have progressed from the tens of pixels of early $\Delta T/T$ experiments through thousands for DMR [3] and SK95 [10], soon tens of thousands for long duration balloon experiments (LDBs) and eventually millions for the MAP [11] and Planck [12] satellites. Finding nearly optimal strategies for data projection, compression and analysis which will allow us to disentangle the primary anisotropies from the Galactic and extragalactic foregrounds and from the secondary anisotropies induced by nonlinear effects will be the key to realizing the theoretically-possible precision on cosmic parameters and so to determine the winners and losers in theory space. Particularly powerful is to combine results from different CMB experiments and combine these with LSS and other observations. Almost as important as the end-product is the application of the same techniques to probing the self-consistency and cross-consistency of experimental results.

Much phenomenology is done using few-parameter local models of $\mathcal{C}_\ell$, e.g., one with a broad-band power $\langle\mathcal{C}_\ell\rangle_B$ and a broad-band tilt $\nu_{\Delta T}$ used for COBE. It has been usual in the COBE literature to denote $1+\nu_{\Delta T}$ by n, inviting confusion with the index for the primordial adiabatic fluctuation power spectrum, $n_s = 1+\nu_s$; for SCDM models with Ω_k=0 and Ω_Λ=0, $\nu_{\Delta T} \approx 0.15 + \nu_s$ over the COBE band. It is evident from Fig. 2 that a single power law is a poor fit to the data when the ℓ-range is enlarged. $\mathcal{C}_\ell$-sequences such as the scalar-only tilted CDM sequence with variable n_s shown in the second panel cover the rise in power suggested by the SK95 data (with $n_s \gtrsim 1$) while still matching the COBE data well, and are therefore of phenomenological as well as obvious theoretical interest.

B. Parameters from the CMB, Current State

Combining CMB anisotropy experiments probing different ranges in ℓ-space improves parameter estimates because of the much extended baseline. Current bandpowers, shown in the upper panel of Fig. 2, broadly follow inflation-based expectations (the SCDM $\mathcal{C}_\ell$ is shown underlying them), but may still include residual signals. Lower panels compress the information into 9 optimal bandpower estimates derived from all of the current data by Jaffe, Knox and I.

Jaffe and I [4] have undertaken full Bayesian statistical analysis of the 4 year DMR [3], SP94 [13] and SK94/SK95 [14,10] data sets, taking into account all correlations among pixels in the data and theory. Other experiments were included by using their bandpowers as independent points with the Gaussian errors shown in Fig. 2. We have shown this approximate method works reasonably well by comparing results derived for DMR+SP94+SK95 with the full analysis with those using just their bandpowers [15].

With current errors on the data, simultaneously exploring the entire parameter space of § IB is not useful, so we restricted our attention to various subregions of $\{\Omega_B h^2, \Omega_{cdm} h^2, \Omega_{hdm} h^2, \Omega_k h^2, \Omega_\Lambda h^2, \nu_s, \nu_t, \sigma_8\}$, such as $\{\sigma_8, n_s, h \,|\, \text{fixed}\, t_0, \Omega_B h^2\}$, where Ω_k=0 and Ω_Λ is a function of ht_0 or Ω_Λ=0 and $\Omega_k > 0$ is a function of ht_0. The age of the Universe, t_0, was chosen to be 11, 13 or 15 Gyrs. A recent estimate for globular cluster ages with the Hipparcos correction is 11.5 ± 1.3 Gyr [16], with perhaps another Gyr to be added associated with the delay in globular cluster formation, so 13 Gyr is a good example. We considered the ranges $0.5 \le n_s \le 1.5$, $0.43 \lesssim h \le 1$, and $0.003 \le \Omega_B h^2 \le 0.05$. Results are mostly shown for the old "standard" nucleosynthesis estimate $\Omega_B h^2 = 0.0125$. We assumed reheating occurred sufficiently late to have a negligible effect on $\mathcal{C}_\ell$, by no means clear. $\mathcal{C}_\ell$'s for sample restricted parameter sequences are shown in Fig. 2. We made use of signal-to-noise compression of the data (by factors of 3) in order to make the calculations of likelihood functions such as $\mathcal{L}(\sigma_8, n_s, h \,|\, \text{fixed}\, t_0, \Omega_B h^2)$ more tractable (without loss of information or accuracy).

The n_s constraints are quite good. If σ_8 is marginalized for the tilted ΛCDM sequence with H_0=50, with DMR only, the primordial index is $n_s = 1.02^{+.23}_{-.25}$ for scalar perturbations only (no gravity waves, ν_t=0) and $1.02^{+.23}_{-.18}$ (with gravity waves and ν_t=ν_s), rather encouraging for the nearly scale invariant models preferred by inflation theory. For the 13 Gyr tilted ΛCDM sequence and $H_0 = 50$ (and $\Omega_\Lambda = 0$) we get $1.18^{+.07}_{-.08}$ for DMR+SK95+SP94, $0.99^{+.04}_{-.03}$ when all of the data are used but SK95 and SP94 (in a bandpower approximation), and $1.02^{+.05}_{-.03}$ when all of the current data are used; for $H_0 = 70$ (and $\Omega_\Lambda = 0.66$), the numbers are quite similar, with all of the data giving $1.00^{+.04}_{-.04}$. And marginalizing over H_0 gives $1.00^{+.05}_{-.04}$. H_0 for fixed age is not that well determined by the CMB data alone. After marginalizing over all n_s, we get $H_0 < 75$ at 1σ, but effectively no constraint at 2σ.

For the DMR4+SK95+SP94 data, the 15 Gyr sequence with $\Omega_B h^2$ fixed at 0.0125 fits better than the 13 Gyr sequence, which in turn fits better than the 11 Gyr sequence for $n_s \le 1$. Ω_B is not that well determined: if we consider just the 13 Gyr sequence with variable Ω_B for $n_s = 1$, $\Omega_B \sim 0.17$ is preferred, if we allow n_s to exceed one then a low Ω_B is preferred (and $n_s = 1.15$); but with all of the CMB data, low Ω_B is preferred for $n_s \ge 1$, high for $n_s < 1$. The strong dependence of the position of the acoustic peaks on Ω_k means that the OCDM sequence is better restricted; e.g., for the 11 Gyr sequence $H_0 \sim 65$ and $\Omega_{tot} \sim .6$ is preferred, with either n_s marginalized or constrained to be 1. For the 13 and 15 Gyr sequences, smaller H_0's but similar Ω_{tot}'s are preferred.

C. Parameters from the CMB+LSS, Current State

The first lesson of Fig. 2 is that, in broad brush stroke, smaller angle CMB data (e.g., SP94, SK95) are consistent with COBE-normalized $\mathcal{C}_\ell$'s for these models. Although the CMB data alone may soon be powerful enough to offer strong selection, this will definitely not diminish the role that combining LSS and CMB data will play. The approach we used in [4] to add LSS information to the CMB likelihood functions was to design prior probabilities for $\Gamma + \nu_s/2$ and $\sigma_8 \Omega_{nr}^{0.56}$, reflecting the current observations, but with flexible and generous non-Gaussian and asymmetric forms to ensure the priors can encompass possible systematic problems in the LSS data. For example, our choice for $\sigma_8 \Omega_{nr}^{0.56}$ was quite flat over the 0.5 to 0.7 range, but fell off below 0.5, although some authors actually prefer such low values.

Using only the 4-year *dmr* data and these priors we get $n_s = 0.72^{+.03}_{-.03}$ with gravity waves (GW), $n_s = 0.53^{+.04}_{-.03}$ without for $H_0 = 50$ TCDM, with values slightly increased when SK95 and SP94 are added. (With $\Omega_{hdm} = 0.2$ of the dark matter in massive neutrinos, we get $n_s = 0.93^{+.03}_{-.04}$ with GW, $n_s = 0.89^{+.07}_{-.09}$ without.) For $H_0 = 70$ and $\Omega_\Lambda = 0.66$, we get $n_s = 0.86^{+.04}_{-.04}$. The preferred Hubble parameter for the $n_s = 1$ sequence is 70 ± 5 ($\Omega_\Lambda \approx 0.66$).

When H_0 (range 50 to 100 for the 13 Gyr sequence) is marginalized, the LSS+DMR+SK95+SP94 data gives $1.12^{+.09}_{-.09}$ with GW and a similar number without GW. When all n_s are marginalized, we obtain $H_0 = 76 \pm 4$ ($\Omega_\Lambda \approx 0.73$) with GW, 72 ± 4 ($\Omega_\Lambda \approx 0.7$) without. When all of the current CMB data is used with the LSS priors, $1.00^{+.05}_{-.04}$ and $H_0 = 72 \pm 3$ ($\Omega_\Lambda \approx 0.7$) are obtained for

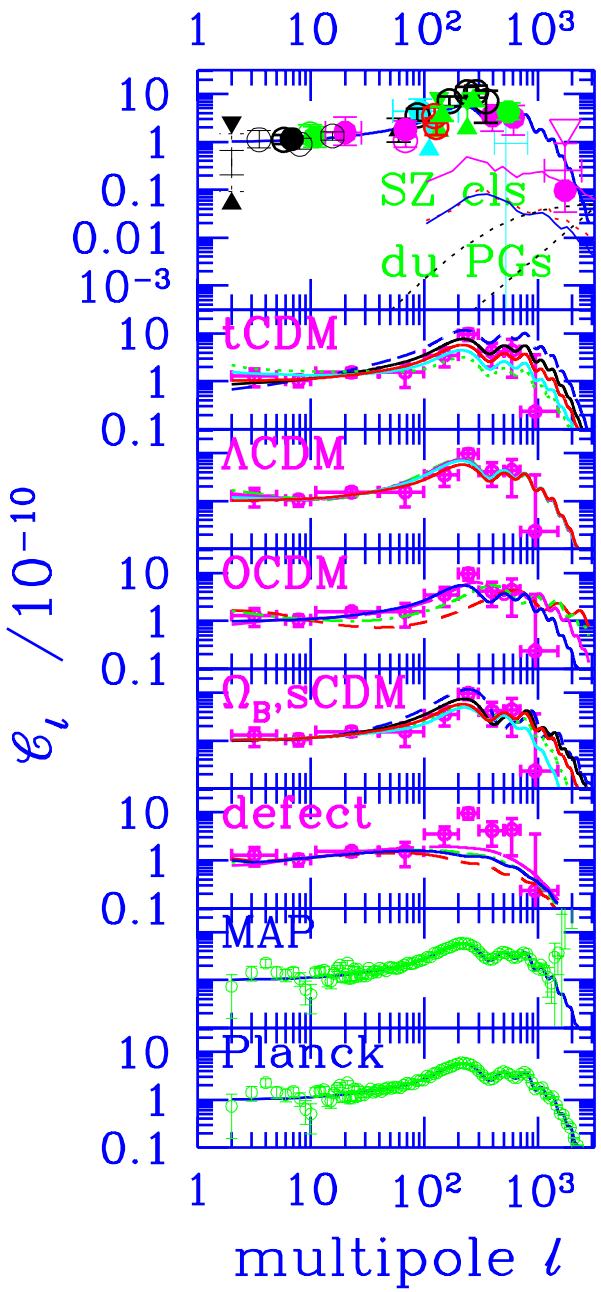

FIG. 2. The anisotropy data for experiments up to March 1997 (upper panel) and optimal combined bandpower estimates (lower panels) are compared with secondary $\mathcal{C}_\ell$'s (upper panel) and various primary $\mathcal{C}_\ell$ sequences. The kinematic SZ $\mathcal{C}_\ell$ is off-scale and the thermal SZ is low *c.f.* the primary $\mathcal{C}_\ell$'s. Dusty emission from early galaxies may lead to high signals, but the power is concentrated at higher ℓ and higher frequency. The next panels are sequences of 13 Gyr models with variations in: (2) n_s, 0.85 to 1.25; (3) Ω_Λ, 0 to 0.87 (H_0 from 50 to 90); (4) Ω_k, 0 to 0.84 (H_0 from 50 to 65); (5) $\Omega_B h^2$, 0.003 to 0.05. (6) shows that sample defect $\mathcal{C}_\ell$'s from Pen, Seljak and Turok [18] do not fare well compared with the current data; $\mathcal{C}_\ell$'s from [19] are similar. Panels 7 and 8 show forecasts of $\mathcal{C}_\ell$ errors for the satellites MAP and Planck.

the GW case, $0.96^{+.07}_{-.05}$ and $H_0 = 70 \pm 3$ without. (If a fixed ratio $\Omega_{hdm}/\Omega_{nr} = 0.2$ for two degenerate massive neutrino species is included, then $n_s \approx 0.97^{+.02}_{-.02}$ and $H_0 \approx 57^{+5}_{-3}$ is obtained, thus slightly preferring $\Omega_\Lambda \sim 0.3$.) For all of the CMB +LSS data, the 13 Gyr open sequence (without massive neutrinos) prefers $\Omega_{tot} \approx 0.6$ and $H_0 \approx 54$. For the 15 Gyr ΛCDM sequence, the result for n_s after marginalization over all $H_0 \geq 43$ (the value for the $\Omega_\Lambda = 0$ model) for all CDM plus LSS is $0.98^{+.04}_{-.03}$ with GW, $0.95^{+.05}_{-.05}$ without; and when n_s is marginalized, $H_0 = 57 \pm 3$ ($\Omega_\Lambda \approx 0.6$) with GW, 54 ± 3 ($\Omega_\Lambda \approx 0.5$) without.

Should these small error bars be taken seriously? They are driven by just the DMR plus LSS results. I would be rather surprised if σ_8 from cluster abundances is drastically revised; and as we have seen, the DMR results are quite robust. The reason the errors are small is typically that the CMB data has a likelihood peaked at high $\sigma_8 \gtrsim 1$, while the LSS one peaks at 0.6 or so, so the product is narrow, but with a small likelihood. This asymmetry is not as pronounced for HCDM models with a light massive neutrino, and the model does not require $\Omega_\Lambda > 0$, but it does help a bit.

D. CMB Constraints on Ultra-large Scale Structure

The "beyond our horizon" land in Fig. 1 is actually partly accessible because long waves contribute gentle gradients to our observables. Constraints on such "global parameters" as average curvature are an example, $d_c > 1.1 H_0^{-1}$, though not yet very restrictive. One may also probe whether a huge bump or deficit in power exists just beyond $k^{-1} \sim H_0^{-1}$, but this has not been much explored. The remarkable non-Gaussian structure predicted by stochastic inflation theory would likely be too far beyond our horizon for its influence to be felt. The bubble boundary in hyperbolic inflation models may be closer and its influence shortly after quantum tunneling occurred could possibly have observable consequences for the CMB. Theorists have also constrained the scale of topology in simple models. We [17] find the torus scale is $d_T/2 > 1.1(2H_0^{-1}) = 6600\,\mathrm{h}^{-1}$ Mpc from DMR for flat equal-sided 3-tori at the 95% confidence limit, slightly better than other groups find since we used full map statistics. The constraint is not as strong if the repetition directions are asymmetric, $> 0.7(2H_0^{-1})$ for 1-tori from DMR. It is also not as strong if more general topologies are considered, e.g., the large class of compact hyperbolic topologies [17].

E. Parameters from the CMB, Future

Quite an industry has developed forecasting how well future balloon experiments (Maxima, Boomerang, ACE, Beast, Top Hat), interferometers (VSA, CBI, VCA) and especially the satellites MAP and Planck could do in measuring the radiation power spectrum and cosmological parameters if foreground contamination is ignored [20–22,12,23,24], and that is what is done here in Table I, using the techniques employed in [23]; similar results have been obtained in [24]. Earlier forecasts made by [22] and [12] were quite influential in the case for MAP and Planck funding. The expected error bars on the power spectrum from MAP and Planck in Fig. 2 show even quite small differences in the theoretical $\mathcal{C}_\ell$'s and thus the parameters can be distinguished.

We assume models have Gaussian-distributed temperature anisotropies. Among the > 17 parameters of § IB, we use a restricted 9 parameter space, 5 densities, $\{\Omega_B, \Omega_{nr}, \Omega_{hdm}, \Omega_k, \Omega_\Lambda\}\mathrm{h}^2$, the Compton depth τ_C, the scalar tilt, n_s, the total bandpower for the experiment $\langle \mathcal{C}_\ell \rangle_B$ in place of $\mathcal{P}_\Phi(k_n)$, and the ratio of tensor to scalar quadrupole powers, $r_{ts} \equiv \mathcal{C}_2^{(T)}/\mathcal{C}_2^{(S)}$, in place of ν_t. r_{ts} is a sensitive function of ν_t, but also depends on $\nu_s - \nu_t$, Ω_Λ, etc. [1]. In this space, recall that $\mathrm{h}^2 = \sum_j (\Omega_j \mathrm{h}^2)$ is a dependent quantity.

Except for the integrated Sachs-Wolfe effect at low ℓ, the angular pattern of CMB anisotropies now is a direct map of the projected spatial pattern at redshift ~ 100, dependent upon the cosmological angle-distance relation, which is constant along a line relating $\Omega_k \mathrm{h}^2$ and $\Omega_\Lambda \mathrm{h}^2$ for fixed $\Omega_{nr}\mathrm{h}^2$. This defines a near-degeneracy between Ω_k and Ω_Λ broken only at low ℓ where the large cosmic variance precludes accurate determination of both parameters simultaneously, and other cosmological observables such as Type I supernovae at high redshift are needed to break this degeneracy.

Error forecasts depend upon the parameters defining the correct underlying theory. In Table I and the lower panels of Fig. 2, untilted SCDM was chosen as the target model, but the values shown are indicative. See [23] for more cases. The Table shows how the forecasts work for DMR, using the average noise in the 53+90+31 GHz map for $\overline{\sigma}_{pix}$, $60\mu K$ per 2.6° pixel. The channel-weighted noise power (first row) is $\overline{C}_\ell = (\overline{\sigma}_{pix}\theta_{pix})^2$. In a 2 parameter tilted sequence, the forecast is for a bandpower with 7% accuracy and n_s to ± 0.20 accuracy, in agreement with the full analysis of § IIB. The number of orthogonal combinations of parameters that could be determined to better than ± 0.1 accuracy was determined by using the full 9 parameter sequences. The NCP numbers are SK95-like, for a 9° radius patch. In combination with DMR, the forecast is that two combinations can be obtained to ± 0.1, in agreement with § IIB.

The third column gives errors forecasted for a LDB experiment (using conservative numbers for the bolometer-based TopHat experiment [25] that took account of excess noise associated with foreground removal). Other balloon bolometer experiments such as Boomerang [26] and MAXIMA [27] should be able to do as well. HEMT-based LDB experiments, such as BEAST [28] using 40 GHz HEMTs, might also achieve similar accuracy. The ℓ-cuts shown for NCP and LDB reflect their limited sky coverage; adding DMR to extend the baseline diminishes the forecasted errors.

We adopt improved specifications especially in beam size, ℓ_s, for MAP [11] and Planck [12] over the original proposal values; these are likely to evolve for Planck. Of the 5 HEMT channels for MAP, we assume the 3 highest frequency channels, at 40, 60 and 90 GHz, will be dominated by the primary cosmological signal (with 30 and 22 GHz channels partly contaminated by bremsstrahlung and synchrotron emission). MAP also assumes 2 years of observing. For Planck, 14 months of observing and current (proposal-modified) values are used. The HEMT-based LFI specifications are significantly improved; the 100, 65, 44 GHz channels, but not the 30 GHz channel, were used. For the bolometer-based HFI, 100, 150, 220 and 350 GHz were used. Dust-contamination will certainly affect the 550 and 850 GHz channels.

These idealized error forecasts do not take into account the cost of separating the many components expected in the data, in particular Galactic and extragalactic foregrounds, but there is currently optimism that the Galactic foregrounds at least may not be a severe problem e.g., [11,12]. There is more uncertainty about the extragalactic foregrounds. We forecast that not far away there will be a day when phenomenological theorists will have optimally-analyzed LDBs/VSA/CBI/VCA/MAP/Planck and delivered the power spectrum and cosmic parameters to wonderful precision. What will it mean? It may not be clear. Take inflation as an example. There will be (undoubtedly optimal) attempts to reconstruct the inflaton's potential, but all of our CMB and LSS observations actually access only a very small region of the potential, and even this will be fuzzily determined if we allow too much freedom in parameter space. Still even a fuzzy glimpse is worth the effort. And if the phenomenology teaches us that non-baroque inflation and defect models fail, the CMB and LSS data will be called upon to guide us to a new theory of how fluctuations are generated.

---

[1] Bond, J.R. (1996) in *Cosmology and Large Scale Structure*, Les Houches Session LX, August 1993, eds. R. Schaeffer J. Silk, M. Spiro & J. Zinn-Justin

Param	DMR	NCP +DMR	LDB +DMR	MAP$^+$ (3ch)	Planck LFI(3)	Planck HFI(4)
$\overline{C}_{D\ell}/10^{-15}$	950	7	1.5	0.77	.10	.0033
f_{sky}	.65	.006	.028	.65	.65	.65
beams: ℓ_s	17	270	400	620	810	1970
ℓ_s		17	17	460	505	1225
ℓ_s				340	350	800
ℓ_s						560
cut: ℓ_{cut}	3	23	12	2	2	2
Orthogonal Parameter Combinations within ε						
$\varepsilon < 0.01$	0/9	0/9	1/9	3/9	3/9	5/9
$\varepsilon < 0.1$	1/9	2/9	4/9	6/9	6/9	7/9
Single Parameter Errors from Marginalizing Others						
$\delta\langle\mathcal{C}_\ell\rangle_B^{1/2}/\langle\mathcal{C}_\ell\rangle_B^{1/2}$	.07	.03	.022	.017	.019	.015
δn_s	.20	.05	.13	.04	.01	.006
δr_{ts}			.89	.24	.13	.09
$\delta\Omega_B h^2/\Omega_B h_0^2$			.23	.05	.016	.006
$\delta\Omega_{nr} h^2/h_0^2$			.33	.10	.04	.02
$\delta\Omega_\Lambda h^2/h_0^2$			.84	.28	.14	.05
$\delta\Omega_{hdm} h^2/h_0^2$			.25	.05	.04	.02
τ_C			.30	.19	.18	.16
$\delta\sigma_8/\sigma_8$			.28	.23	.21	.18
$\delta\mathcal{P}_\Phi^{1/2}/\mathcal{P}_\Phi^{1/2}$			.24	.19	.17	.15
$\delta\Omega_k h^2/h_0^2$			.14	.04	.02	.007
$\delta h/h$			.29	.14	.05	.02

TABLE I. Sample DMR, NCP, LDB, MAP, Planck parameter errors, assuming SCDM is the true theory. The errors are of course sensitive to which model we choose. $\overline{C}_{D\ell}$ is the all-channel noise, assumed to be uniform for all maps. The channel-dependent Gaussian-beam filter ℓ_s is related to the beam *fwhm* by $\theta_{fwhm} \approx 8090\ell_s^{-1}$ arcmin. Relative errors are quoted for h, $\Omega_B h^2$, and the amplitudes $\langle\mathcal{C}_\ell\rangle_B^{1/2}$, σ_8 and $\mathcal{P}_\Phi^{1/2}(k_n)$ (the early universe gravitational potential amplitude for scalar adiabatic perturbations). The $\Omega_\Lambda h^2$ numbers are determined with $\Omega_k h^2$ fixed, and the $\Omega_k h^2$ numbers are determined with $\Omega_\Lambda h^2$ fixed, because of the angle-distance near-degeneracy; the other parameters are insensitive to fixing either, or neither. NCP denotes earth-based observations covering a 9° radius patch, similar to SK95. For DMR, NCP+DMR and LDB+DMR weak restrictions were placed on allowed variation of the parameters, using prior probabilities to multiply the likelihood functions. The DMR and DMR+NCP forecasts compare favourably with current errors. The LDB parameters are based upon ten days of observing with the bolometer-based TopHat experiment with 65% of a 24° diameter patch assumed usable. The usable sky fraction for DMR, 65%, was adopted for the satellites. The specific choices for MAP and Planck are described in the text. The forecasted errors obviously represent a great leap forward from current errors and from what is conceivable with non-CMB probes.

(Elsevier Science Press, Amsterdam), pp. 469-674.

[2] Bond, J.R. (1994) in *Relativistic Cosmology*, Proc. 8th Nishinomiya-Yukawa Memorial Symposium, ed. M. Sasaki, (Universal Academy Press, Tokyo), pp. 23-55.

[3] Bennett, C., Banday, A.J., Gorski, K.M., Hinshaw, G., Jackson, P., Keegstra, P., Kogut, A., Smoot, G.F., Wilkinson, D.T. & Wright, E.L. (1996) Ap. J. Lett., **464**, 1-4.

[4] Bond, J.R. & Jaffe, A. (1996) in *Microwave Background Anisotropies*, Proceedings of the XXXI Rencontre de Moriond, ed. F.R. Bouchet, Edition Frontières, Paris, pp. 197-208, astro-ph/9610091; (1997) CITA preprint.

[5] Peacock, J.A. (1996) preprint astro-ph/9608151.

[6] Bertschinger, E., Bode, P., Bond, J.R., Coulson, D., Crittenden, R., Dodelson, S., Efstathiou, G., Gorski, K., Hu, W., Knox, L., Lithwick, Y., Scott, D., Seljak, U., Stebbins, A., Steinhardt, P., Stompor, R., Souradeep, T., Sugiyama, N., Turok, N., Vittorio, N., White, M., Zaldarriaga, M. (1995) ITP workshop on *Cosmic Radiation Backgrounds and the Formation of Galaxies*, Santa Barbara.

[7] Seljak, U. & Zaldarriaga, M. (1996) Ap. J.**469**, 437-444.

[8] Fixsen, D.J., Cheng, E.S., Gales, J.M., Mather, J.C., Shafer, R.A. & Wright, E.L. (1997) Ap. J.**473**, 576-587.

[9] Bond, J.R. & Myers, S. (1996) Ap. J. Supp. **103**, 1-79.

[10] Netterfield, C.B., Devlin, M.J., Jarosik, N., Page, L. & Wollack, E.J. (1997) Ap. J.**474**, 47.

[11] MAP experiment home page, http://map.gsfc.nasa.gov

[12] Bersanelli, M., Bouchet, F.R., Efstathiou, G., Griffin, M., Lamarre, J.M., Mandolesi, N., Norgaard-Nielson, H.U., Pace, O., Polny, J., Puget, J.L., Tauber, J., Vittorio, N. & Volonte, S. (1996) COBRAS/SAMBA, The Phase A Study for an ESA M3 Mission, preprint; Planck home page, http://astro.estec.esa.nl/SA-general/Projects/Cobras/cobras.html

[13] Gundersen, J.O., Lim, M., Staren, J., Wuensche, C.A., Figueiredo, N., Gaier, T. C., Koch, T., Meinhold, P.R., Seiffert, M.D., Cook, G., Segale, A. & Lubin, P.M. (1995) Ap. J. Lett., **443**, L57-60.

[14] Netterfield, C.B., Jarosik, N., Page, L. & Wilkinson, D. (1995) Ap. J. Lett. **455**, L69-72.

[15] Jaffe, A.H., Knox, L. & Bond, J.R. (1997) preprint astro-ph/9702109

[16] Chaboyer, B., Demarque, P., Krauss, L.M. & Kernan, P.J. (1997) preprint astro-ph/9706128

[17] Bond, J.R., Pogosyan, D. & Souradeep, T. (1996) preprint astro-ph/9702212.

[18] Pen, Ue-Li, Seljak, U. & Turok, N. (1997) preprint astro-ph/9704165.

[19] Allen, B., Caldwell, R.R., Dodelson, S., Knox, L.,

Shellard, E.P.S. & Stebbins, A. (1997) preprint astro-ph/9704160.
[20] Knox, L. (1995) Phys. Rev. D **52**, 4307-4318.
[21] Tegmark, M. & Efstathiou, G. (1996) M.N.R.A.S. 281, 1297-1314.
[22] Jungman, G., Kamionkowski, M., Kosowsky, A. & Spergel, D.N. (1996) Phys. Rev. Lett. **76**, 1007-1010.
[23] Bond, J.R., Efstathiou, G. & Tegmark, M. (1997) M.N.R.A.S., in press, astro-ph/9702100.
[24] Zaldarriaga, M., Spergel, D. & Seljak, U. (1997) Ap. J., in press, astro-ph/9702157.
[25] TopHat home page, http://cobi.gsfc.nasa.gov/msam-tophat.html
[26] Boomerang home page, http://astro.caltech.edu/ mc/boom/boom.html
[27] MAXIMA home page, http://physics7.berkeley.edu/group/cmb/gen.html
[28] ACE/Beast home page, http://www.deepspace.ucsb.edu/research/Sphome.html